Modelling of Transient Discharges Along a Sub-mm Air-Solid Dielectric Interface Under Fast-rising Ramp Voltages

Timothy Wong*, Igor Timoshkin, Scott MacGregor, Mark Wilson, and Martin Given

Department of Electronic and Electrical Engineering
University of Strathclyde
Glasgow, Scotland, UK
*timothy.wong@strath.ac.uk

Abstract—Fast-rising high voltage impulses, gas-dielectric interfaces, and electrode topologies which generate significant electric field nonuniformity are features often encountered within pulsed power applications. The consideration of pre-breakdown and breakdown processes, especially those across gas-solid interfaces in divergent electric fields, is important for the operation and optimization of different pulsed power and low temperature plasma systems. In this work, primary ionization waves across a sub-mm solid-gas interface have been modelled in a 2D approximation using the drift-diffusion approach. They have been initiated from a needle electrode of 80 micrometers radius, partially embedded inside a solid dielectric, and partially exposed to air. The gap separation studied in this work was 250 micrometers, in which positive and negative ramp voltages were applied with rising slopes of 25, 16.67, 12.5, and 10 kV/ns, emulating the rising edge of impulses with different rates of voltage rise. The resulting spatiotemporal evolution of the electric field and nonthermal plasma channel has been obtained and discussed. The obtained results can help in the development of pulsed power and nonthermal plasma systems, and further contributes to the fundamental understanding of the mechanisms driving gas-solid interfacial discharge under fast impulses with high *dV/dt*.

Index Terms—nonthermal plasma, gas-solid interface, pulsed power applications, low temperature plasma, streamer discharge
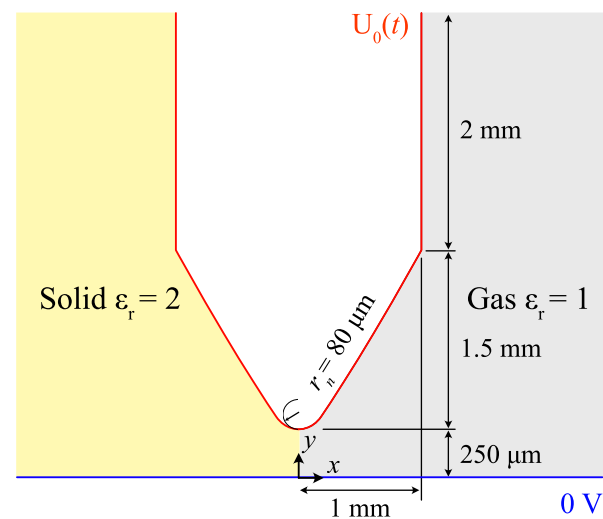
Fig. 1. Diagram of the 2D needle-plane simulation domain with labelled dimensions. The full extent of the domain extends beyond the boundary of the figure.

I. Introduction

Low temperature plasma (LTP) technology has gathered significant interest in recent times. Examples include surface treatment and cleaning [1], environmental applications [2], and chemical processing [3]. Equally, the role of LTPs during the pre-breakdown phase in gas insulated systems also attracted interest from the power, pulsed power, and microelectronic industries. The understanding of pre-breakdown ionization fronts under certain conditions, such as fast-rising electric fields, at gas-solid interfaces, or in compact non-standard systems such as microelectromechanical devices (MEMS), remains incomplete. As such, a deeper understanding of LTPs

under non-standard conditions may be highly beneficial to a wide range of current and future technologies.

In this work, computational simulations have been conducted that investigated the effects of fast-rising voltages on the characteristics of primary ionization fronts, developed within an embedded needle-plane electrode gap with sub-millimeter separation, and along a dielectric surface.

II. Simulation Conditions

A. Geometry Configuration

The simulation was configured following Fig. 1, consisting of a hyperbolic segment with curvature 80 μm representing the high voltage (HV) needle electrode, placed 250 μm above a grounded plane. A solid dielectric with relative permittivity $\varepsilon_r = 2$ (reflective of a typical value found in commonly used polymeric HV insulation) occupies the left half of the inter-electrode space, while the right half is filled with a 80/20 % N_2/O_2 gas mixture (synthetic air).

1

B. Extended Hydrodynamic Model

To model the initiation of an ionization wave and the subsequent development of the LTP channel, the hydrodynamic approach using the StrAFE [4] library was employed. Briefly, this included the particle balance equations given by:

$$\partial_t n_i + \nabla \cdot \vec{\Gamma}_i = S_i, \tag{1}$$

where n_i, $\vec{\Gamma}_i$ and S_i are the particle concentration, total flux, and summed sources and sinks of the charged species i, respectively, and where ∂_t is the time derivative. The total flux is given by the sum of advective and diffusive components,

$$\vec{\Gamma}_i = -\mathrm{sgn}(q_i) n_i \mu_i \nabla \varphi - D_i \nabla n_i, \tag{2}$$

where the transport properties of species i is characterized by its mobility μ_i and diffusion coefficient D_i. Additionally, q_i is the signed charge and φ is the scalar electric potential, which is coupled to (1) through the Poisson equation:

$$-\nabla \cdot (\varepsilon \nabla \varphi) = \sum_i q_i n_i, \tag{3}$$

and where ε is the dielectric permittivity. The set of reactants used in this work were $i = \{e, O_2^+, N_2^+, O_4^+, N_4^+, O_2^+ N_2, O_2^-\}$, and where the implemented reactions alongside their rates are listed in Table I. Photoionization was included using Zheleznyak's model [5] solved using the three-parameter Helmholtz approximation following Bourdon *et al.* [6], while the local mean energy approximation (LMEA) was also used, with the electron energy density dynamically computed following:

$$\partial_t n_\varepsilon + \nabla \cdot \vec{\Gamma}_\varepsilon = \bar{e}\vec{\Gamma}_e \cdot \nabla \varphi - \sum_R \Delta E_R, \tag{4}$$

where n_ε and $\vec{\Gamma}_\varepsilon$ are the electron energy density and total energy flux, respectively, while ΔE_R is the total energy change in electron energy during reaction R, and $\bar{e}$ is the elementary charge.

C. Boundary Conditions

On the HV needle electrode, a time-dependent Dirichlet condition for the electric potential was applied of the form:

$$U_0(t) = \frac{dV}{dt} t \tag{5}$$

in order to emulate the application of a linearly ramping voltage rising at a rate of *dV/dt*. The ground (planar) electrode was held constant at zero volts. For both electrodes on the side exposed to the gas, and for the solid dielectric surface, the Neumann condition:

$$\vec{\Gamma}_i \cdot \hat{n} = |n_i \mu_i \nabla \varphi| + \frac{1}{2} v_{th,i} n_i \tag{6}$$

was applied, which is a reduced version of the conditions proposed by Hagelaar, de Hoog, and Kroesen [7] neglecting particle reflection and secondary emission. Here $v_{th,i}$ is the thermal velocity of species i. To account for the surface

TABLE I
TABLE OF CHEMICAL REACTIONS AND REACTION RATES USED IN THE PRESENT MODEL. $f(\bar{\varepsilon})$ INDICATES THAT THE REACTION RATE IS A FUNCTION OF THE ELECTRON ENERGY.

R	Reaction	Rate	Unit	Ref.
R_1	$e + N_2 \rightarrow N_2^+ + e + e : 15.6$ eV	BOLSIG+	$m^3 s^{-1}$	[8]
R_2	$e + N_2 \rightarrow N_2^+ + e + e : 18.8$ eV	BOLSIG+	$m^3 s^{-1}$	[8]
R_3	$e + O_2 \rightarrow O_2^+ + e + e$	BOLSIG+	$m^3 s^{-1}$	[8]
R_4	$e + O_2 + O_2 \rightarrow O_2^- + O_2$	$f(\bar{\varepsilon})$	$m^6 s^{-1}$	[9]
R_5	$N_2^+ + N_2 + M \rightarrow N_4^+ + M$	5×10^{-41}	$m^6 s^{-1}$	[9]
R_6	$N_4^+ + O_2 \rightarrow O_2^+ + N_2 + N_2$	2.5×10^{-16}	$m^3 s^{-1}$	[9]
R_7	$N_2^+ + O_2 \rightarrow O_2^+ + N_2$	6×10^{-17}	$m^3 s^{-1}$	[9]
R_8	$O_2^+ + N_2 + N_2 \rightarrow O_2^+ N_2 + N_2$	9×10^{-43}	$m^6 s^{-1}$	[9]
R_9	$O_2^+ N_2 + N_2 \rightarrow O_2^+ + N_2 + N_2$	4.3×10^{-16}	$m^3 s^{-1}$	[9]
R_{10}	$O_2^+ N_2 + O_2 \rightarrow O_4^+ N_2$	1×10^{-15}	$m^3 s^{-1}$	[9]
R_{11}	$O_2^+ + O_2 + M \rightarrow O_4^+ + M$	2.4×10^{-42}	$m^6 s^{-1}$	[9]
R_{12}	$e + O_4^+ \rightarrow O_2 + O_2$	$f(\bar{\varepsilon})$	$m^3 s^{-1}$	[9]
R_{13}	$e + O_2^+ \rightarrow O + O$	$f(\bar{\varepsilon})$	$m^3 s^{-1}$	[9]
R_{14}	$O_2^- + O_4^+ \rightarrow 3O_2$	1×10^{-13}	$m^3 s^{-1}$	[9]
R_{15}	$O_2^- + O_4^+ + M \rightarrow 3O_2 + M$	2×10^{-37}	$m^6 s^{-1}$	[9]
R_{16}	$O_2^- + O_2^+ + M \rightarrow O_2 + O_2 + M$	2×10^{-37}	$m^6 s^{-1}$	[9]
R_{17}	$e + N_2 \rightarrow e + N_2 + \gamma$	Zheleznyak.	–	[5]
R_{18}	$\gamma + O_2 \rightarrow e + O_2^+$	Zheleznyak.	–	[5]

charging phenomenon due to the particle influx at the gas-solid interface, the jump condition:

$$\varepsilon \nabla \varphi \cdot \vec{n} = \sigma_s \tag{7}$$

was applied, where in the absence of secondary or photoemission, the surface charge σ_s evolves according to the boundary-directed fluxes:

$$\partial_t \sigma_s = \bar{e} \sum_i \mathrm{sgn}(q_i)\vec{\Gamma}_i \cdot \hat{n}. \tag{8}$$

It is noted that volume conduction through the solid was neglected, as it was deemed to have negligible effect under the timescales considered in this work.

D. Simulation Settings

H-type adaptive mesh refinement (AMR) and a sub-ps adaptive timestep was used, as described in [4]. Time integration was performed to second-order accuracy using the Crank-Nicolson scheme, and with the simulation computed on an 18-core workstation computer equipped also with 64 GB memory.

III. RESULTS AND DISCUSSION

Voltages of both positive and negative polarity have been studied, at rates of rise of *dV/dt* = 25, 16.67, 12.5, and 10 kV/ns. In all cases, ionization waves developed due to the enhanced field at the needle tip, caused by the curvature of the needle electrode and by the triple junction formed at the solid-gas-electrode intersection. This primary ionization front propagated and bridged the inter-electrode gap within 1 ns, scaling with *dV/dt*. The appearance of the ionization wave was similar between all values of *dV/dt*, albeit shifted in time according to the rate of rise. However, there were some distinctive features which differed between positive and negative fronts, discussed below.
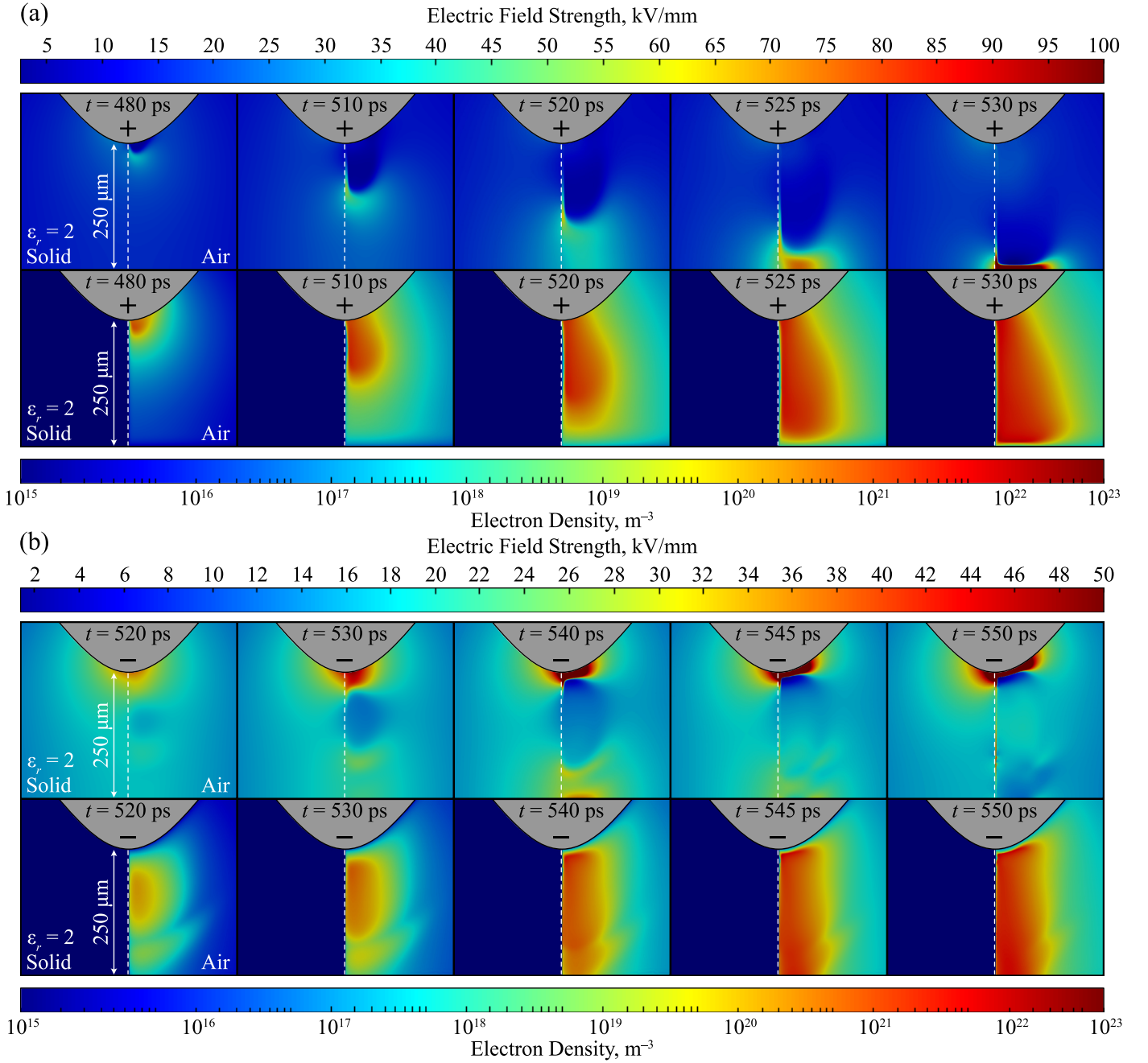
(a)

(b)

Fig. 2. Electric field distribution and electron density over time for (a) positive energization (b) negative energization at 10 kV/ns across the sub-mm dielectric surface. Domain is cropped to only show the region in the near vicinity of the discharge.

A. Positive Energization

Fig. 2(a) shows the time evolution of the ionization wave under a positive ramp voltage (10 kV/ns). The color plots on the top row show the electric field strength while those on the bottom row show the electron density. Prior to the first column (t = 480 ps), space charge developed at the triple-junction region at the needle tip leads to sufficient field distortion at approximately 470 ps, which initiates the propagation of the front. The front then rapidly accelerates down the surface. It also expands away from the surface, driven by an intense

electric field developed within the sheath distance between the plasma channel and the dielectric surface. Upon reaching the cathode, the plasma spreads out across the cathode sheath, completing the channel connection which now resembles a cone.

B. Negative Energization

Fig. 2(b) shows the time evolution of the ionization wave under a negative ramp voltage, in the same format as Fig. 2(a). It should be noted that the times at which the plots of
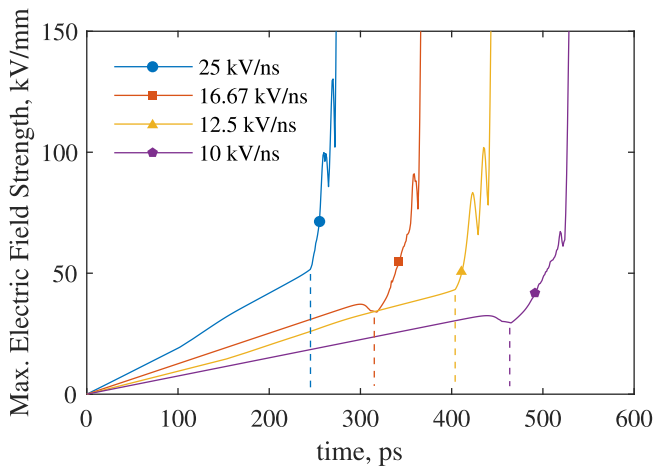
3

Fig. 3. Maximum electric field over time for positive ionization waves (positive energization of the HV needle electrode) and at different rates of voltage rise.

Fig. 4. Electric field magnitude moving the from the needle tip toward the plane, at a distance $x = 5$ μm away from the dielectric surface, and at various timesteps for a 16.67 kV/ns signal. Negative energization of the HV needle electrode.

Fig. 2(b) have been recorded differ from those of Fig. 2(a), as the negative ionization front took longer to develop than the positive. Prior to the formation of the ionization front in the gap, a wave of electrons has been observed to propagate away from the needle due to electron drift, indicating the initial development of a cathode sheath. As a result, the main ionization front develops at a distance away from the needle tip, which in the short sub-mm gap considered here, means that the offset distance is significant, and the front begins its propagation almost at the halfway point within the inter-electrode gap at around 520 ps. The subsequent field enhancement in the space between the newly formed ionization front and the plane electrode causes a sudden and rapid increase in the electron density ahead of the original front (as can be seen in Fig. 2(b), 530 ps). The combination of these two regions completes the plasma channel, which in contrast to the positive case, does not appear conical in nature but more of a direct bridge between the two electrodes.

C. Electric Field and Electron Density

Fig. 3 shows the maximum recorded electric field strength inside the domain over time, and for all simulated rates of voltage rise for the positive case. During the initial stage, the maximum electric field rises linearly due to the absence of any space charge induced field distortion. The moment of initiation of an ionization wave is indicated by a sharp and sudden change in the maximum electric field strength with time, as annotated in Fig. 3 by dashed lines. The electric field continues to climb during the short (several tens of picoseconds) propagation stage of the ionization front, before a second rapid increase in field indicates the collision with the planar electrode and formation of the cathode sheath. The time between these two moments is also indicative of the average propagation velocity of the front, which was observed to increase with higher values of dV/dt.
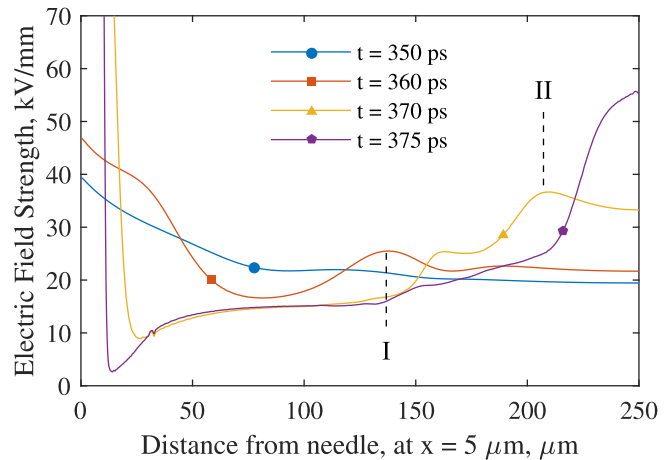
The same field characteristic has not been plotted for negative energization because of the early formation of the cathode sheath over the needle electrode. This resulted in the maximum electric field remaining at the same location (inside the cathode sheath, at the needle electrode) for the entire simulation, and is therefore of little use to characterize the negative front behavior. Additionally, since the main ionization front develops at a significant distance away from the needle (closer to the plane than the needle in most cases), it is perhaps unsuitable to speak of the 'propagation' of the front (in the classical sense of the front moving down the gap), since the front does not really traverse from one electrode to the other. Rather, and as shown in Fig. 2(b), the development of the plasma channel under negative energization is more akin to the appearance of an electron density almost mid-gap, which expands in both directions toward cathode and anode, eventually forming the complete channel.

As the domain is asymmetrical, Fig. 4 plots the electric field magnitude along the line $x = 5$ μm between $y = 250$ and $y = 0$ μm for the case of a negative front at 16.67 kV/ns (approximating the location of the maximum electric field during the propagation of the surface ionization front, and according to the coordinates of Fig. 1, where (0, 0) lies on the plane electrode). Note that other values of dV/dt have not been shown since they were characteristically similar, just shifted in time. Four timesteps have been included, which correspond to the moment of initiation ($\sim$350 ps) to the moment of electrode contact ($\sim$375 ps). Due to the shortness of the gap combined with the cathode sheath distance, the negative ionization fronts evolved rather differently to their positive counterparts. On Fig. 4, the moment labelled (I) demarcates the position where the first ionization front developed, with the reduced electric field magnitude behind this point indicating the beginnings of the plasma channel. However, since this front developed closer to the plane (anode) than the cathode, the field was also

rapidly enhanced between the original position of the front (I) and the plane, producing the head of a secondary front at (II). For times after moment (II), and since the field within the whole gap is now strongly enhanced, the plasma channel rapidly develops across the gap.

For higher values of dV/dt, it was also observed that the density of active species in the developed plasma positively correlated with dV/dt. This is explained simply by the additional overvoltage which was possible with higher dV/dt, which led to an overall higher electric field, intensifying the ionization and reaction processes.

IV. CONCLUSIONS

In summary, the present work has computationally modelled fast transient ionization fronts in an air-filled sub-mm needle-plane-dielectric gap, under positive and negative ramp voltages. From the obtained results, it has been found that there are key differences in the development of primary ionization waves between polarities. This includes differences in the way the waves are initiated, and differences in how the final plasma channel bridges the inter-electrode gap. Analyses over ramp voltages of different dV/dt also indicated a positive dependence between the front velocity and plasma density with voltage rise of rise. Results from this investigation may be of value to pulsed power and low temperature plasma applications, and further contribute toward the understanding of fast ionization fronts in non-standard, fast-rising, and nonuniform field conditions. In future, this work is planned to be extended to include different gases of interest, or for similar analyses to be conducted under mm or cm gaps. The investigation of the effects of secondary emission and photoemission in sub-mm gaps would also be beneficial to attain a fuller understanding of LTPs under these conditions.

REFERENCES

[1] D. Mihailova, J. van Dijk, G. Hagelaar, P. Belenguer, P. Guillot, "Modeling of Low Temperature Plasma for Surface and Airborne Decontamination," IEEE Trans. Plasma Sci., vol. 42, no. 10, pp. 2760-2761, Oct. 2014.

[2] M. Okubo, Y. Hiroyasu, and T. Kuroki, "Ion Cluster Formation by Nonthermal Plasma Induced by Pulse Corona Discharge Toward Indoor Air Cleaning," IEEE Trans. Ind. Appl., vol. 56, no. 5, pp. 5480-5488, Jul. 2020.

[3] R. Aerts, W. Somers, and A. Bogaerts, "Carbon Dioxide Splitting in a Dielectric Barrier Discharge Plasma: A Combined Experimental and Computational Study," ChemSusChem, vol. 8, no. 4, pp. 702-716, Feb. 2015.

[4] T. Wong, I. Timoshkin, S. MacGregor, M. Wilson, and M. Given, "The Design of a Python Library for the Automatic Definition and Simulation of Transient Ionization Fronts," IEEE Access, vol. 11, pp. 26577-26592, Mar. 2023.

[5] M. B. Zheleznyak, A. K. Mnatsakanyan, and S. V. Sizykh, "Photoionization of nitrogen and oxygen mixtures by radiation from a gas-discharge," High Temp., vol. 20, no. 3, pp. 357-362.

[6] A. Bourdon, V. P. Pasko, N. Y. Liu, S. Célestin, P. Ségur, and E. Marode, "Efficient models for photoionization produced by non-thermal gas discharges in air based on radiative transfer and the Helmholtz equations," Plasma Sources Sci. Technol., vol. 16, no. 3, p. 656, Aug. 2007.

[7] G. J. M. Hagelaar, F. J. de Hoog, and G. M. W. Kroesen, "Boundary conditions in fluid models of gas discharges," Phys. Rev. E, vol. 62, no. 1, p. 1452, Jul. 2000.

[8] G. J. M. Hagelaar and L. C. Pitchford, "Solving the Boltzmann equation to obtain transport coefficients and rate coefficients for fluid models," Plasma Sources Sci. Technol., vol. 14, no. 4, p. 722, Oct. 2005.

[9] S. V. Pancheshnyi and A. Y. Starikovskii, "Two-dimensional numerical modelling of the cathode-directed streamer development in a long gap at high voltage," J. Phys. D: Appl. Phys., vol. 36, no. 21, p. 2683, Oct. 2003.